


**Atomic ionization driven by the quantized electromagnetic field in a Fock state**I. A. Ivanov<sup>1,\*</sup> and Kyung Taec Kim<sup>1,2,†</sup><sup>1</sup>*Center for Relativistic Laser Science, Institute for Basic Science, Gwangju 61005, Korea*<sup>2</sup>*Department of Physics and Photon Science, GIST, Gwangju 61005, Korea* (Received 17 June 2020; revised 20 July 2020; accepted 7 August 2020; published 24 August 2020)

We consider ionization of an atom by the electromagnetic field in a Fock state  $|N\rangle$ : An eigenvector of the operator  $\hat{N}_{k,\lambda} = \hat{a}_{k,\lambda}^\dagger \hat{a}_{k,\lambda}$  of the number of photons in the mode  $\mathbf{k}, \lambda$ . We treat the electromagnetic field in a quantized way, which allows us to obtain the photon picture of the strong field ionization. We obtain, in particular, probability distributions for the number of absorbed photons in the process of strong field ionization for atomic systems governed by short-range and Coulomb potentials.

DOI: [10.1103/PhysRevA.102.023117](https://doi.org/10.1103/PhysRevA.102.023117)**I. INTRODUCTION**

It has been realized since the pioneering work by Reiss [1] that even for mundane field intensities of the order of  $10^{14}$  W/cm<sup>2</sup>, the description of atomic or molecular photoionization based on the nonrelativistic time dependent Schrödinger equation (TDSE) may have its limitations. It was shown in [1] that relativistic effects may play significant role in the process of atomic or molecular photoionization. Of particular interest is the so-called tunneling regime of ionization. Even for infrared (IR) laser fields with intensity of the order of  $10^{14}$  W/cm<sup>2</sup>, the relativistic nondipole effects are visible in the experimentally observed photoelectron spectra [2]. An IR photon possesses a small momentum, but a large number of photons participating in the process of tunneling ionization [3] deliver appreciable momentum to the ionized electron. Nondipole effects accompanying multiphoton processes in this regime of ionization have been studied extensively experimentally [2,4] and theoretically [5–12]. Relativity also introduces effects related to the electron spin into the theory of strong field ionization. A strong spin asymmetry can be observed in the above-threshold ionization (ATI) process [10,13]. Development of free-electron lasers (FELs) [14–16] opens up a possibility of the experimental study of the relativistic effects for multiphoton processes in the domain of high photon energies, where the nondipole effects due to finite photon momentum can be expected to be particularly important. That this is indeed the case was shown in [17,18].

Development of laser techniques [14–16,19,20] has allowed reaching superhigh intensities (of the order of  $10^{23}$  W/cm<sup>2</sup>) of laser radiation, and there are projects envisaging reaching yet higher intensities of the order of  $10^{26}$  W/cm<sup>2</sup> [21]. Such intensities are still below the so-called Schwinger limit (intensity of the order of  $10^{29}$  W/cm<sup>2</sup>) when effects such as photon-photon interaction and electron-positron pair production become important. There are ways,

however, to effectively enhance the pair production [21–23], making it possible to observe this effect at lower intensities. Theoretical description of such phenomena is provided by quantum electrodynamics (QED). QED enjoys the status of an extremely accurate physical theory which has made numerous spectacular predictions of the experimentally measured quantities such as the anomalous magnetic moment of the electron or the Lamb shift of the hydrogen energy levels, agreeing with experiment with an unprecedented accuracy. These achievements have been attained by summing the contributions of several leading orders of the QED perturbation theory expansion. The perturbation theory, while providing spectacularly accurate results in many cases is, however, not always applicable. It fails, in particular in strong electromagnetic fields, where a nonperturbative theoretical framework is required.

Comparing to the more traditional treatment of the strong field ionization based either on a numerical solution of the TDSE or other methods such as the well-known strong field approximation (SFA) [24–27] or Floquet theory [28], QED brings into consideration the effects due to the fact that in QED both electrons and photons are described as quantum fields [29]. We will consider in this work the effects due to the quantum nature of the electromagnetic field (i.e., its photon character). In other words, we will consider below quantum evolution of an atomic system in the presence of a quantized electromagnetic field with an intensity of the order of  $10^{14}$  W/cm<sup>2</sup>. As far as the atomic system is concerned, we will treat it quantum mechanically, using a suitably modified TDSE as described below. Such an approach implies that we neglect the quantum field character of the electronic part of the problem, in particular the essentially many-body character of the quantum field describing electrons. In the present context this means that we neglect completely the processes such as pair creation, which is, of course, quite legitimate for the field intensities we use below.

The paper is organized as follows. In Sec. II we describe theoretical and numerical techniques we will use. Our results and conclusions are presented in the Secs. III and IV, respectively. Atomic units with  $\hbar = 1$ ,  $e = 1$ ,  $m =$

\*igorivanov@ibs.re.kr

†kyungtaec@gist.ac.kr

1, and  $c \approx 137.036$  (here  $e$  and  $m$  are charge and mass of the electron,  $c$  the speed of light) are used throughout the paper.

## II. THEORY

We recapitulate briefly, following the work [30], the method we employ in the present work to account for the quantum field character of the electromagnetic field. We will apply this method below to analyze distribution of the absorbed photons in the strong field ionization process.

The quantized vector potential can be written as [30,31]

$$\hat{\mathbf{A}}(\mathbf{r}, t) = \sum_{\mathbf{k}, \lambda} \sqrt{\frac{2\pi c^2}{\omega V}} (\mathbf{e}_{\mathbf{k}, \lambda} \hat{a}_{\mathbf{k}, \lambda} e^{-i\omega t + i\mathbf{k} \cdot \mathbf{r}} + \text{H.c.}). \quad (1)$$

It is assumed in Eq. (1) that the electromagnetic field is quantized in a finite volume  $V$ , so summation in Eq. (1) runs through the discrete set of modes characterized by wave vector  $\mathbf{k}$  and polarization direction  $\mathbf{e}_{\mathbf{k}, \lambda}$ ;  $\hat{a}_{\mathbf{k}, \lambda}$  and  $\hat{a}_{\mathbf{k}, \lambda}^\dagger$  are annihilation and creation operators with usual bosonic commutation relations. The combined Hilbert space of the system atom + field is the tensor product  $\mathcal{H}_{\text{atom}} \otimes \mathcal{H}_{\text{field}}$ , where  $\mathcal{H}_{\text{atom}}$  and  $\mathcal{H}_{\text{field}}$  are atomic and photon Hilbert spaces. A convenient basis in the photon subspace  $\mathcal{H}_{\text{field}}$  is provided by the Fock states  $|N\rangle$ : eigenvectors of the operator  $\hat{N}_{\mathbf{k}, \lambda} = \hat{a}_{\mathbf{k}, \lambda}^\dagger \hat{a}_{\mathbf{k}, \lambda}$  of the number of photons in the mode  $\mathbf{k}, \lambda$ . We will consider below only one mode of the field, corresponding to linear polarization in the  $z$  direction and a particular photon frequency; we will omit henceforth, therefore, subscripts  $\mathbf{k}, \lambda$  in the formulas.

Let us choose some Fock state  $|N\rangle$  with large  $N$ . The representation described in [30] consists of mapping of the Fock states  $|N+m\rangle$  ( $m \geq -N$ ) on the set of exponential functions of angle  $\theta$ :

$$|N+m\rangle = e^{im\theta}. \quad (2)$$

Using this mapping, the photon part of the Hilbert space  $\mathcal{H}_{\text{field}}$  can be realized as a space of the functions  $f(\theta)$ , defined on the interval  $\theta \in (0, 2\pi)$ , with the scalar product

$$\langle f|g\rangle = \frac{1}{2\pi} \int_0^{2\pi} f^*(\theta)g(\theta) d\theta. \quad (3)$$

Correspondingly, to preserve the usual properties  $a|N\rangle = \sqrt{N}|N-1\rangle$ ,  $a^\dagger|N\rangle = \sqrt{N+1}|N+1\rangle$  of the creation and annihilation operators, they should be realized as operators acting on the functions depending on  $\theta$  in the following ways:

$$\begin{aligned} a &= e^{-i\theta} \left( N - i \frac{\partial}{\partial \theta} \right)^{\frac{1}{2}}, \\ a^\dagger &= \left( N - i \frac{\partial}{\partial \theta} \right)^{\frac{1}{2}} e^{i\theta}. \end{aligned} \quad (4)$$

Other representations of annihilation and creation operators as differential operators are also possible [32]; Eq. (4) is particularly convenient in the strong field limit  $N \rightarrow \infty$ . In this limit, which will interest us, one may write  $\lim_{N \rightarrow \infty} a = e^{-i\theta} \sqrt{N}$ ,  $\lim_{N \rightarrow \infty} a^\dagger = e^{i\theta} \sqrt{N}$ . Using these asymptotic relations the quantized vector potential (1) can be written in the limit

$N \rightarrow \infty$  as

$$\hat{\mathbf{A}}(\mathbf{r}, t) = \sqrt{\frac{2N\pi c^2}{\omega V}} (\mathbf{e}_z e^{-i\omega t + i\mathbf{k} \cdot \mathbf{r} - i\theta} + \text{H.c.}). \quad (5)$$

We note that under the asymptotic large- $N$  approximation made above we lose the ability to describe certain processes, such as spontaneous emission of photons. The amplitudes of the processes of the spontaneous emission of photons acquire an additional factor of  $1/N$  compared to the stimulated emission or absorption processes, and are, therefore, beyond the accuracy of this asymptotic approximation. It is, however, the processes of stimulated emission and absorption which are of interest to us in the present work, and which can be considered in the leading order of  $1/N$  expansion.

Though the expression in (5) looks like the classical expression for the vector potential, it is still an operator in the photon part of the Hilbert space  $\mathcal{H}_{\text{field}}$  because of the dependence on the angle  $\theta$ . To complete the description we need an atom-field interaction Hamiltonian:

$$\hat{H}_I(t) = \frac{1}{2c} \hat{\mathbf{p}} \hat{\mathbf{A}} + \frac{1}{2c} \hat{\mathbf{A}} \hat{\mathbf{p}} + \frac{1}{c^2} \hat{\mathbf{A}}^2. \quad (6)$$

The QED time-evolution propagator  $\hat{U}(t, 0)$  driving evolution of the system atom + field in the combined Hilbert space  $\mathcal{H}_{\text{atom}} \otimes \mathcal{H}_{\text{field}}$  can then be written in a formally closed form using the Dyson time-ordering operator  $\hat{T}$  [33]:

$$\hat{U}(t, 0) = \hat{T} \exp \left( -i \int_0^t \hat{H}(t') dt' \right), \quad (7)$$

where  $\hat{H}(t) = \hat{H}_{\text{atom}} + \hat{H}_I(t)$  and  $\hat{H}_{\text{atom}} = \frac{\hat{\mathbf{p}}^2}{2} + V(r)$  is atomic Hamiltonian taken in the nonrelativistic approximation. Note that we do not need to include the field Hamiltonian in Eq. (7) because the evolution under the field Hamiltonian is already included in the expression (1) for the vector potential. In other words, the representation we use here is obtained from the Schrödinger representation of the quantum equations of motion (in which both atomic and field operators do not depend on time) by means of the unitary transformation  $\exp(-i\hat{H}_{\text{field}}t)$  generated by the field Hamiltonian  $\hat{H}_{\text{field}}$ .

Using the representation (2), expression (5), and the definition (3) of the scalar product in  $\mathcal{H}_{\text{field}}$ , it is easy to see that in the limit of large  $N$  the matrix elements of the QED time-evolution propagator  $\hat{U}(t, 0)$  taken between the Fock states can be written as [30]

$$\langle N+m|\hat{U}(t, 0)|N\rangle = \frac{1}{2\pi} \int_0^{2\pi} \hat{U}(t, 0; \theta) e^{-im\theta} d\theta. \quad (8)$$

Here,  $\hat{U}(t, 0; \theta)$  is an operator acting in the atomic Hilbert space  $\mathcal{H}_{\text{atom}}$  only. This operator satisfies the familiar atomic time-dependent Schrödinger equation [30]

$$\begin{aligned} i \frac{\partial \hat{U}(t, 0; \theta)}{\partial t} &= \left( \hat{H}_{\text{atom}} + \frac{1}{2c} \hat{\mathbf{p}} \mathbf{A}(\theta) + \frac{1}{2c} \mathbf{A}(\theta) \hat{\mathbf{p}} \right. \\ &\quad \left. + \frac{1}{2c^2} \mathbf{A}(\theta)^2 \right) \hat{U}(t, 0; \theta), \end{aligned} \quad (9)$$

where  $\mathbf{A}(\theta)$  is now a classical field,

$$\begin{aligned} \mathbf{A}(\mathbf{r}, t, \theta) &= \sqrt{\frac{2N\pi c^2}{wV}} (e_z e^{-i\omega t + i\mathbf{k}\cdot\mathbf{r} - i\theta} + \text{H.c.}) \\ &= A_0 \cos(\omega t + \theta - \mathbf{k}\cdot\mathbf{r}), \end{aligned} \quad (10)$$

with the amplitude  $A_0 = \sqrt{\frac{8N\pi c^2}{\omega V}}$ . All we have to do, therefore, to find the matrix elements of the complete QED propagator between the different Fock states is to find the atomic propagator  $\hat{U}(t, 0; \theta)$  in Eq. (9) as a function of the phase  $\theta$ , and to perform the  $\theta$  integration as prescribed by Eq. (8). We will apply the formula (8) for the QED propagator for the case when an atom, initially (in the distant past) in the ground state, interacts with the quantized electromagnetic field. More specifically, we will be interested in the photon distribution in the distant future. To describe such a situation we will, as is customarily done [34], supply the interaction Hamiltonian with a cutoff function, making the interaction Hamiltonian vanish both in the distant past and the distant future. We will discuss the question of the proper choice of the cutoff function in more detail below.

Using Fock states (2) centered around a given (and large  $N$ ) the wave function of the complete system atom + field can be represented as

$$\Phi(t) = \sum_{m=-N}^{\infty} \phi_m(t) \otimes |N+m\rangle, \quad (11)$$

where  $\phi_m(t)$  are vectors from the atomic Hilbert space  $\mathcal{H}_{\text{atom}}$ . Assuming that initial state of the system atom + field is  $\phi_0 \otimes |N\rangle$  (where  $\phi_0$  is the ground atomic state), and using the representation (8) for the QED propagator, one obtains

$$\phi_m = \frac{1}{2\pi} \int_0^{2\pi} \hat{U}(t, 0; \theta) e^{-im\theta} \phi_0 d\theta, \quad (12)$$

with  $P(n, t) = |\phi_{-n}(t)|^2$  giving the probability of detecting the field in a state  $|N-n\rangle$  at the moment  $t$ . Note that, for the sake of convenience, we chose the signs in the definition of  $P(n, t)$  in such a way that positive argument  $n$  corresponds to the absorption of  $n$  photons from the field, while negative values of  $n$  correspond to the stimulated emission of  $n$  photons. Another useful formula one can derive from the Eqs. (11) and (12) is the representation of the atomic density matrix at time  $t$ , which can be obtained by taking a partial trace with respect to photon degrees of freedom, with the result [30]

$$\begin{aligned} \hat{\rho}_{\text{atom}}(t) &= \sum_m \langle N+m | \Phi(t) \rangle \langle \Phi(t) | N+m \rangle \\ &= \frac{1}{2\pi} \int_0^{2\pi} \hat{U}(t, 0; \theta) \hat{\rho}_{\text{atom}}(0) \hat{U}^\dagger(t, 0; \theta) d\theta, \end{aligned} \quad (13)$$

where  $\hat{\rho}_{\text{atom}}(0) = |\phi_0\rangle\langle\phi_0|$  is the initial atomic density matrix. Equation (13) shows concisely that, to take into account the fact that the phase of the field is completely undermined in the Fock state of the field, one must perform a certain ‘‘phase average’’ as prescribed by the equation.

To compute  $P(n, t)$  in Eq. (12) we proceed as follows. As we noted above, with respect to action on the vectors from the atomic Hilbert space  $\mathcal{H}_{\text{atom}}$ ,  $\hat{U}(t, 0; \theta)$  behaves like an ordinary quantum mechanical propagator, satisfying the quantum-

mechanical TDSE (9) with the classical field  $\mathbf{A}(\mathbf{r}, t, \theta)$  in Eq. (10). To find the vector  $\phi_m$  in (12) we should, therefore, first find a set of atomic wave functions  $\phi(t, \theta)$  describing evolution of the atom in the presence of the classical field with different phases (10),

$$\begin{aligned} i \frac{\partial \phi(t, \theta)}{\partial t} &= \left( \hat{H}_{\text{atom}} + \frac{1}{2c} \hat{\mathbf{p}} \mathbf{A}(\theta) + \frac{1}{2c} \mathbf{A}(\theta) \hat{\mathbf{p}} \right. \\ &\quad \left. + \frac{1}{2c^2} \mathbf{A}(\theta)^2 \right) \phi(t, \theta) \end{aligned} \quad (14)$$

with the initial condition that  $\phi(t, \theta)$  is the ground atomic state in the distant past, and then compute  $\phi_m$  in Eq. (12) as

$$\phi_m = \frac{1}{2\pi} \int_0^{2\pi} \phi(t, \theta) e^{-im\theta} d\theta. \quad (15)$$

In the following we will neglect in Eq. (14) the spatial dependence of the vector potential, using thus the dipole approximation, which is legitimate for the the field parameters we will be considering below. The solution of the TDSE equations (14) is quite straightforward (albeit somewhat computationally demanding since we have to solve a large number of evolution equations for different phases  $\theta$ ). The actual number of phases  $\theta$  to consider depends on the ionization regime, which can be conveniently characterized by two dimensionless parameters [27,35]: The multiquantumness parameter  $K = I/\omega$  and the Keldysh parameter [3,24]  $\gamma = \omega\sqrt{2I}/E_0$  (where  $\omega$  and  $E_0$  are frequency and strength of the laser field and  $I$  is the ionization potential of the target system in atomic units). Below we will consider regimes with  $K \gg 1$  and different values of the Keldysh parameter, ranging from  $\gamma > 1$  (multiphoton ionization) to  $\gamma \lesssim 1$  (tunneling regime of ionization). In both cases the atom undergoing ionization absorbs a considerable number of photons from the field. According to the definition of the Fock states (2), absorption of the photons from the field corresponds to negative  $m$  values. It is clear from Eq. (15) that, to compute accurately the integral in this formula for large negative values of  $m$  for which integrand rapidly oscillates, we need to use an adequately accurate quadrature rule. In our calculations we used the Gauss quadrature rule with up to the total of  $M_g = 141$  points (for the largest field strength we consider below), with  $\theta$  values distributed in the interval  $(0, 2\pi)$ . The TDSE was solved for these  $\theta$  values using the numerical procedure for solving the TDSE for an atom driven by a strong classical electromagnetic field, which we employed previously in calculations of atomic and molecular ionization processes [36–39] and which we described in detail elsewhere [40].

Having obtained solutions of the TDSE for the  $\theta$  values at the Gauss quadrature grid points, we can compute the integral in Eq. (15) and hence the probability  $P(n)$ . Because of the unitarity of the evolution driven by the QED Hamiltonian (6) we have, of course,  $\sum_{n=-\infty}^{+\infty} P(n, t) = 1$  at all times. We will be primarily interested below in the process of absorption of photons; i.e., with the sign convention we adopted, we will consider  $P(n)$  with positive  $n$ . We will also be interested below in the normalized probability distribution  $Q(n, t)$  of the absorbed photons. This distribution is just a conditional probability of absorbing  $n$  photons from the field provided at least one photon has been absorbed, and it coincides with

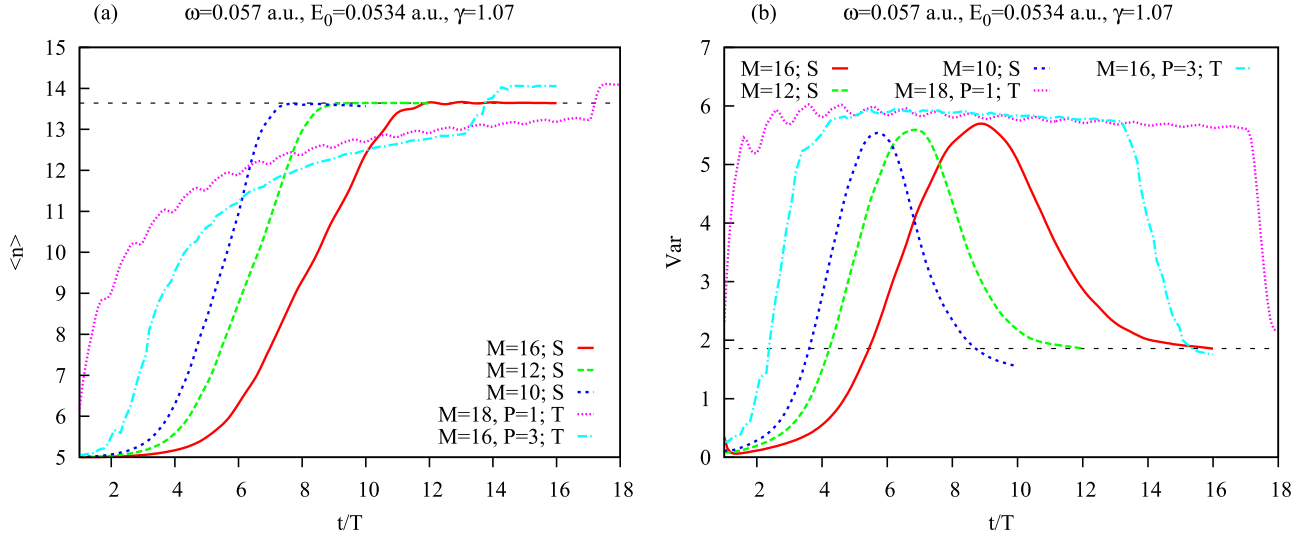


FIG. 1. Expectation value and variance of the distribution of the absorbed photons for different envelope functions in the expression (16) for the vector potential.

$P(n, t)$  for  $n \geq 1$  up to a normalization factor which ensures that  $\sum_{n=1}^{+\infty} Q(n, t) = 1$  at all times.

### III. RESULTS

Before presenting the results we will discuss the possible effect of the cutoff envelope function which we used in the calculations. As we noted above, when solving the TDSE we have to introduce a cutoff envelope function  $f(t)$ , so that the actual expression for the vector potential in the classical interaction Hamiltonian differs from the right-hand side of Eq. (10) by the presence of the envelope  $f(t)$ :

$$A(t) = A_0 f(t) \cos(\omega t + \theta). \quad (16)$$

Introducing the envelope function is necessary both for computational reasons (we cannot propagate the TDSE on very long time intervals, and we wish to avoid the effects of the sudden switch on of the interaction) and for the more fundamental reason of gauge invariance. The minimal coupling we use in the expression for the interaction QED Hamiltonian (6) is not the only possible gauge which can be used for the description of the atom-field interaction. A QED analog [32,41] of the quantum mechanical length gauge can also be used for this purpose. The results obtained become gauge independent after the interaction is switched off. We must ensure, of course, that the choice of the envelope function we use in calculations is adequate in the sense that its particular shape does not affect appreciably the conclusions we will draw from the results we present below. We begin this section, therefore with a detailed study of this question.

#### A. Choice of the envelope function

We show below the results obtained for two specific envelope functions in the expression (16) for the vector potential. Both envelope functions assume nonzero values in the interval  $(0, MT)$  [here  $M$  is an integer and  $T$  is the optical cycle corresponding to the base frequency of the pulse (16)]. We

will report below results of the the calculations using base frequencies of  $\omega = 0.057$  a.u. (corresponding to the wavelength of 800 nm) and  $\omega = 0.172$  (wavelength of 265 nm). The first envelope function (we will call it the S type) is the familiar  $\sin^2$  envelope often employed in the calculations of atomic ionization processes:

$$f(t) = \sin^2\left(\frac{\pi t}{MT}\right), \quad t \in (0, MT), \quad (17)$$

and the second, the ‘‘trapezoidal’’ envelope (we will call it the T type) is defined on the interval  $(0, MT)$  by the equations

$$f(t) = \begin{cases} \alpha(t), & t \in (0, PT), \\ 1, & t \in (PT, MT - PT), \\ \alpha(MT - t), & t \in (MT - PT, MT), \end{cases} \quad (18)$$

where  $PT$  is the switching interval, and the switching function  $\alpha(t)$  is a third-order polynomial  $\alpha(t) = 3t^2/(PT)^2 - 2t^3/(TP)^3$ , monotonically growing on the switching interval, which ensures continuity of the vector potential and its first derivative at  $t = PT$  and  $t = MT - PT$ . We can vary switching interval  $PT$  by changing parameter  $P$ .

In Fig. 1 we show two important characteristics of the normalized probability distribution  $Q(n, t)$  of the absorbed photons: Its expectation value  $\langle n(t) \rangle = \sum_{n=1}^{\infty} nQ(n, t)$  and variance  $\text{Var}(n, t) = \sum_{n=1}^{\infty} Q(n, t)(n - \langle n \rangle)^2$ . We choose a particular value  $E_0 = 0.0534$  a.u. of the effective field strength  $E_0$  which, by Eq. (10), is related to the number of photons in the initial Fock state  $|N\rangle$  of the radiation field as  $E_0 = \sqrt{8N\omega\pi c^2/V}$ . The atom in this calculation was a model one-electron system with a short-range potential

$$W(r) = -1.903 \frac{e^{-r}}{r}. \quad (19)$$

This potential supports only one bound state of  $s$  symmetry, with the ionization potential equal to that of the hydrogen atom. This choice was made to make a sensible comparison with the case when Coulomb interaction is present, which we will consider later.



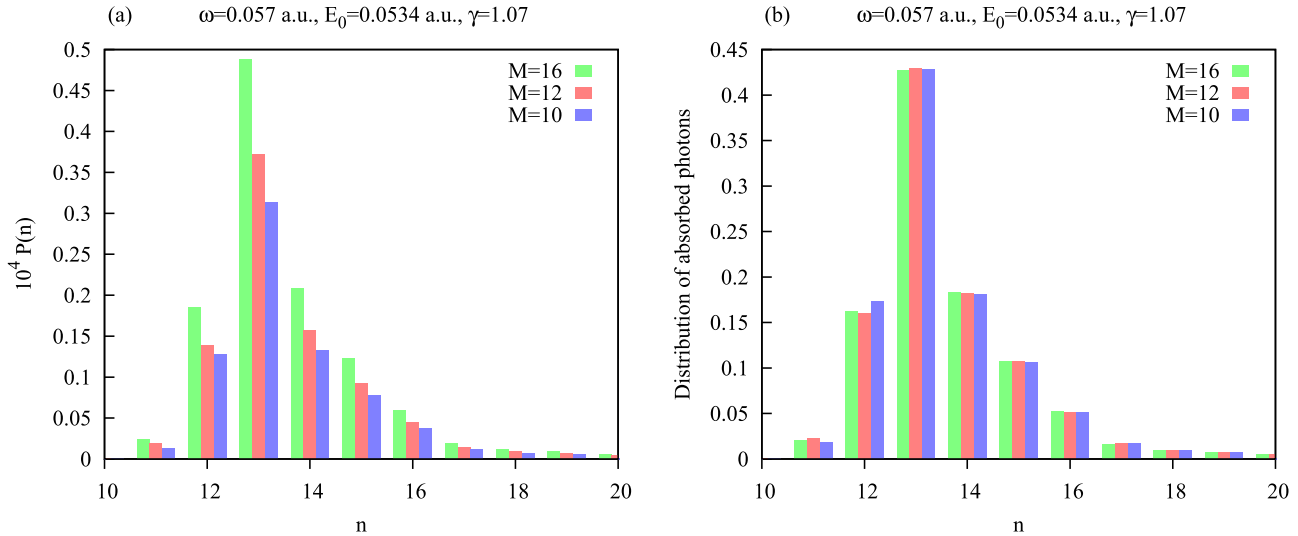


FIG. 2. Distribution  $P(n)$  and the normalized probability distribution  $Q(n)$  of the absorbed photons for the same field parameters as in Fig. 1, obtained at the end of the pulse (17) with the pulse durations of  $M = 10$ ,  $M = 12$ , and  $M = 16$  optical cycles.

In Fig. 1 we show results obtained for the different choices of the envelope functions. We employ the system of notation we introduced in Eqs. (17) and (18). Thus, for instance, the calculation in Fig. 1 marked as  $M = 16$ ; S uses the  $\sin^2$  envelope (17) with the total pulse duration  $16T$  (here, we remind,  $T = 2\pi/\omega$  is an optical cycle corresponding to the base frequency  $\omega = 0.057$  a.u. we use in this work). The calculation marked as  $M = 18$ ,  $P = 1$ ; T employs the envelope function (18), with the total pulse duration of  $18T$ , and the pulse being switched on and off on the intervals  $(0, T)$  and  $(17T, 18T)$ . One can see that despite the completely different shapes and durations, the values of the expectation values and variances agree quite well at the end of the pulse, which is the physically interesting region. This transition to the asymptotic values (marked in black dots in Fig. 1) occurs somewhat smoother and faster for the  $\sin^2$  envelope function, probably because of its more “adiabatic” character, as compared to the trapezoidal envelope. As one can see, for the  $\sin^2$  envelope (17) the expectation value and the variance reach their asymptotic (infinite future) values rather early in the course of the evolution. Comparison of the calculations with  $M = 12$ ; S and  $M = 16$ ; S in Fig. 1 show that they give practically identical predictions for the asymptotic infinite future values for both the expectation value and the variance of the distribution of the absorbed photons. Further confirmation of the statement that using the calculation with  $M = 12$ ; S we obtain at the end of the pulse distributions which practically coincide with the distributions in the “infinite future” is provided by the results shown in Fig. 2. The figure shows the results for the probability distribution  $P(n)$  and the normalized probability distribution  $Q(n)$  of the absorbed photons for the same field parameters as in Fig. 1, obtained at the end of the pulse (17) with different durations. Figure 2(a) shows that the probabilities  $P(n)$  expectedly grow with the duration of the pulse. More important for our purposes are the results presented in Fig. 2(b), where the normalized probability distributions  $Q(n)$  are shown for different durations of the  $\sin^2$  envelope pulse. One can see that the distributions obtained for  $M = 10$ ,

$M = 12$ , and  $M = 16$  are practically identical, thus justifying the conclusion we have made above that the absorbed photon distribution obtained at the end of the pulse (17), with the total pulse duration of  $M = 12$  optical cycles can, with good accuracy, be considered as the distribution obtained in the distant future for the atom-field interaction switched off adiabatically. We have used, therefore, the envelope (17) with  $M = 12$  in all the calculations reported below. This choice appears to give accurate enough results for the asymptotic large time distributions of the absorbed photons, on one hand, and it can be treated with relative ease numerically, as we do not have to integrate the TDSE on very long time intervals.

Following this strategy, which we outlined above and illustrated for the field strength of  $E_0 = 0.0534$  a.u., we performed a series of calculations for the base frequency  $\omega = 0.057$  a.u., varying the effective field strength  $E_0$ . These results are reported below.

### B. Distributions of absorbed photons in the multiquantum multiphoton and tunneling regimes.

In Fig. 3 we show distribution  $P_n$  for different effective field strengths for the model atom with the short-range potential (19).

We can compare the results we obtain with the results following from the well-known formula for the differential ionization probability of the SFA theory [27]:

$$\frac{dP}{d\Omega d\epsilon_p} = \sum_{n>n_0} R(\mathbf{p}) \delta(\epsilon_p + I_p + U_p - n\omega), \quad (20)$$

where  $n_0 \geq N_{\min} = (I_p + U_p)/\omega + 1$ , the factor  $R(\mathbf{p})$  can be computed analytically [27],  $I_p$  is ionization potential of the target system, and ponderomotive energy  $U_p = E_0^2/4\omega^2$  for the linearly polarized pulse. The sum on the right-hand side of Eq. (20) often receives interpretation in terms of the absorbed photons, with integral  $\int R(\mathbf{p}) d\Omega$ ,  $\epsilon_p = n\omega - I_p - U_p$  giving the probability of absorbing  $n$  photons from the field. Analogous expressions involving sums of the energy delta

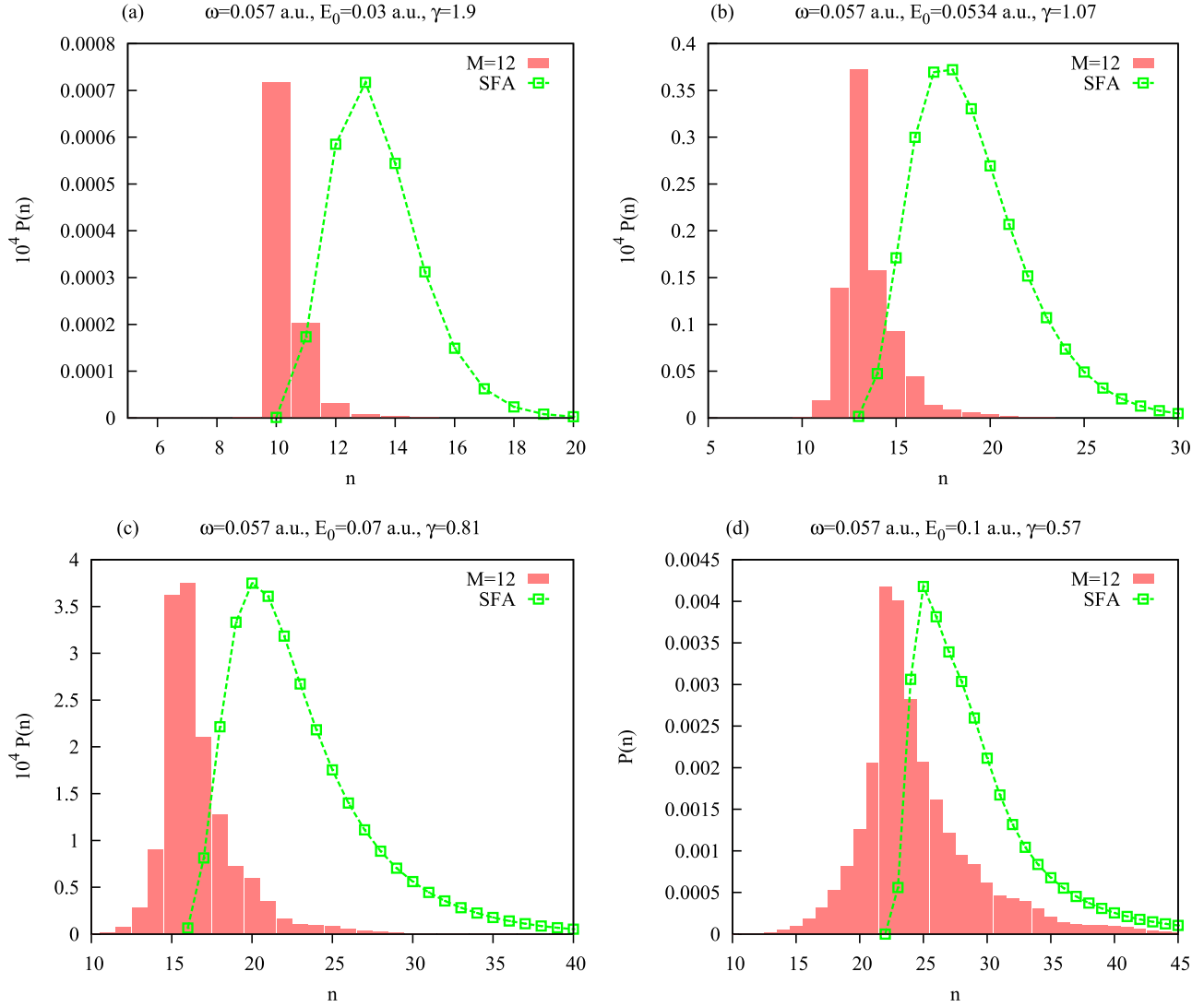


FIG. 3. Distribution  $P(n)$  (red) and the SFA estimate (green dots) for different effective field strengths for the model atom with the short-range potential (19), obtained at the end of the pulse (17) with  $M = 12$  optical cycles.

functions centered at a discrete set of energy values arise in other analytic approaches to the strong field ionization problem, such as the Perelomov-Popov-Terentiev [42] method or an approach developed in [25,26].

This interpretation is, however, partly misleading. Quoting [27], the discreteness of the electron spectrum in Eq. (20) is a consequence of the laser field periodicity only [Eq. (20) has been obtained for the monochromatic laser field], and does not rely, in any way, on the concept of photons. To express it differently, and perhaps more generally, let us note that in the SFA and related approaches, Eq. (20) and its analogs are obtained using an approximation for the electron's wave function [27,35], i.e., only the wave function of an atom is considered. For the description of the system atoms + photons in terms of a wave function, we must, of course, take the photon part of the Hilbert space into consideration, as the method we use in the present work allows us to do. The atom in the complete picture including photons cannot be described by a wave function, but only by a reduced density matrix [30,32].

Nevertheless, the comparison between the photon absorption probabilities obtained in our calculation and given by the SFA estimate might be instructive. We present such a comparison in Fig. 3 by showing the SFA predictions for the distribution of the absorbed photons. We normalized the SFA curve so that both our results and the SFA distribution had maxima of equal magnitude. Figure 3 shows that the most probable number of absorbed photons is larger for the SFA distributions. This feature is most prominent for lower field strengths, the difference in positions of the maxima of the two distributions becoming smaller with increasing field strength. The SFA distribution is also typically wider than the distribution  $P_n$  we obtain, the difference in widths also becoming less pronounced for higher field strengths.

One might be tempted to relate the distributions of the number of absorbed photons to the Poisson distribution. Indeed, this distribution, which describes the probability distribution for a number of events occurring with constant rate on a given interval of time [32], seems to be a good candidate for the model of ionization driven by the field in a Fock state

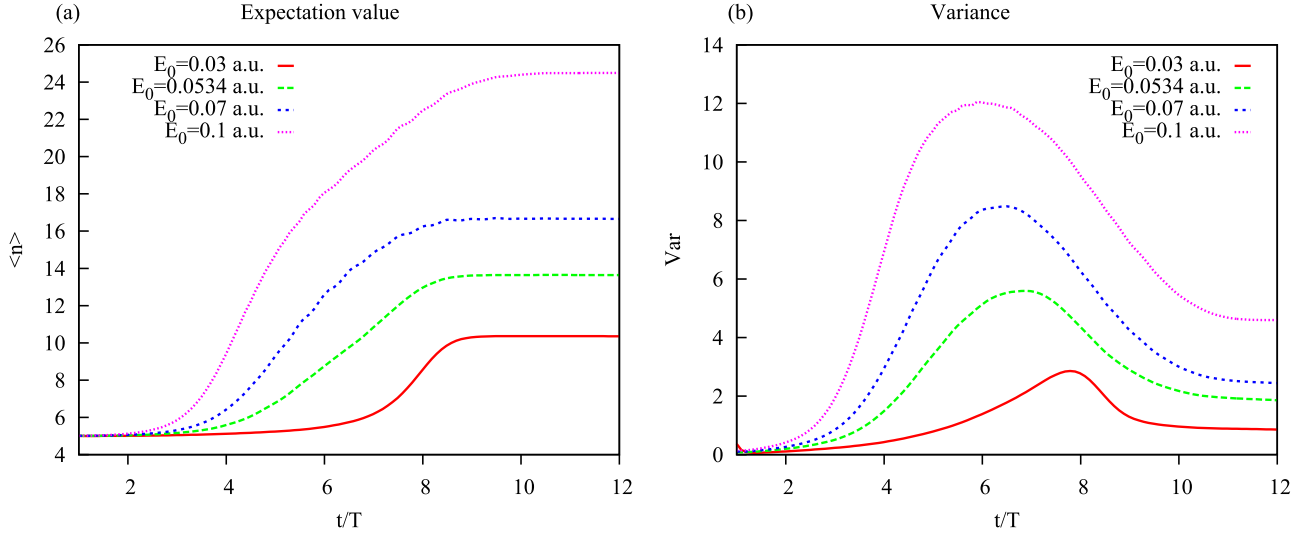


FIG. 4. Expectation value and variance of the distribution of the absorbed photons  $Q(n, t)$  as functions of time for the atomic system governed by the short-range interaction (19).

$|N\rangle$ ). Since the phase of the field is completely undetermined in the Fock state  $|N\rangle$ , which is an eigenstate of the photon number operator, ionization in this case can be pictured as a suitable average over all possible phases of the field [30], as encapsulated by Eq. (15). One might try to represent the effects of such a phase average as ionization with a constant rate, which would lead to the Poisson distribution. That, however, is not the case. That the SFA distribution for the number of absorbed photons derived from Eq. (20) is distinctly non-Poissonic is known [35,43]. Our results also show the non-Poissonic character of this distribution. That can be clearly seen from Fig. 4, where we show characteristics (expectation values and variances) of the normalized probability distribution  $Q(n, t)$  of the absorbed photons for different field strengths as functions of time for the atomic system governed by the short-range interaction (19). We observe essentially the same behavior as shown in Fig. 1: Both expectation value and variance tend to the limiting values, which we interpret as the values of these quantities in the infinite future when the interaction is off. Figure 4 clearly shows non-Poissonic character of  $Q(n, t)$  for any interval  $(0, t)$ . Variance for the Poisson distribution should be equal to the expectation value [32], an equality which is clearly not satisfied by the curves in Fig. 4.

More detailed information about development of the photon number distributions for different effective field strengths is provided by Fig. 5, which shows how the distributions  $P(n, t)$  develop in time before reaching their asymptotic form for different field strengths.

The results we presented so far were obtained for a model atom governed by the short-range potential (19). This was done to obtain a more clear photon picture of the ionization process, which is not influenced by the photon absorption due to the excitation processes [the short-range potential (19) supports only one bound state]. Comparison with the SFA photon distribution derived from the Eq. (20) is also more appropriate in the case of the short-range interaction.

We performed, using the same strategy we employed for the model atom governed by the short-range interaction (19), calculations of the absorbed photons probability distribution  $P(n)$  for the hydrogen atom with Coulomb potential. Results are shown in Fig. 6. While the most probable numbers of the absorbed photons in the cases of the short-range and Coulomb potentials are approximately equal, an obvious difference between the distributions in Figs. 6 and 3 is the far longer tail of the distribution in the Coulomb case. Two mechanisms can be responsible for the formation of this tail. In the case of the finite-range interaction, such as (19), when an ionized electron escapes the range of the action of the atomic potential its motion is practically free. A free electron, as is well known, cannot absorb a photon. In the case of the short-range interaction, therefore, the process of the photon absorption is effectively confined to the time interval when electron is inside the range of the atomic potential. In the infinite-range Coulomb case this restriction is lifted, and electron can absorb a larger number of photons, which leads to a longer distribution tail. Another process which may lead to absorption of a larger number of photons in the case of the Coulomb potential is the photoexcitation process, which is absent in the case of the potential (19) supporting only one bound state.

## IV. REMARKS AND PROSPECTS

### A. Mapping onto the Floquet representation

The present approach can be connected to the well-known Floquet formalism. Let us assume that the total wave function of the system of interacting atom and field at time  $t$  is represented as an expansion (11) over the complete set of the Fock states. In the following it will be more convenient to use the Schrödinger representation, so evolution of the system is given by

$$i \frac{\partial \Phi(t)}{\partial t} = (\hat{H}_{\text{atom}} + \hat{H}_I + \hat{H}_{\text{field}}) \Phi(t). \quad (21)$$

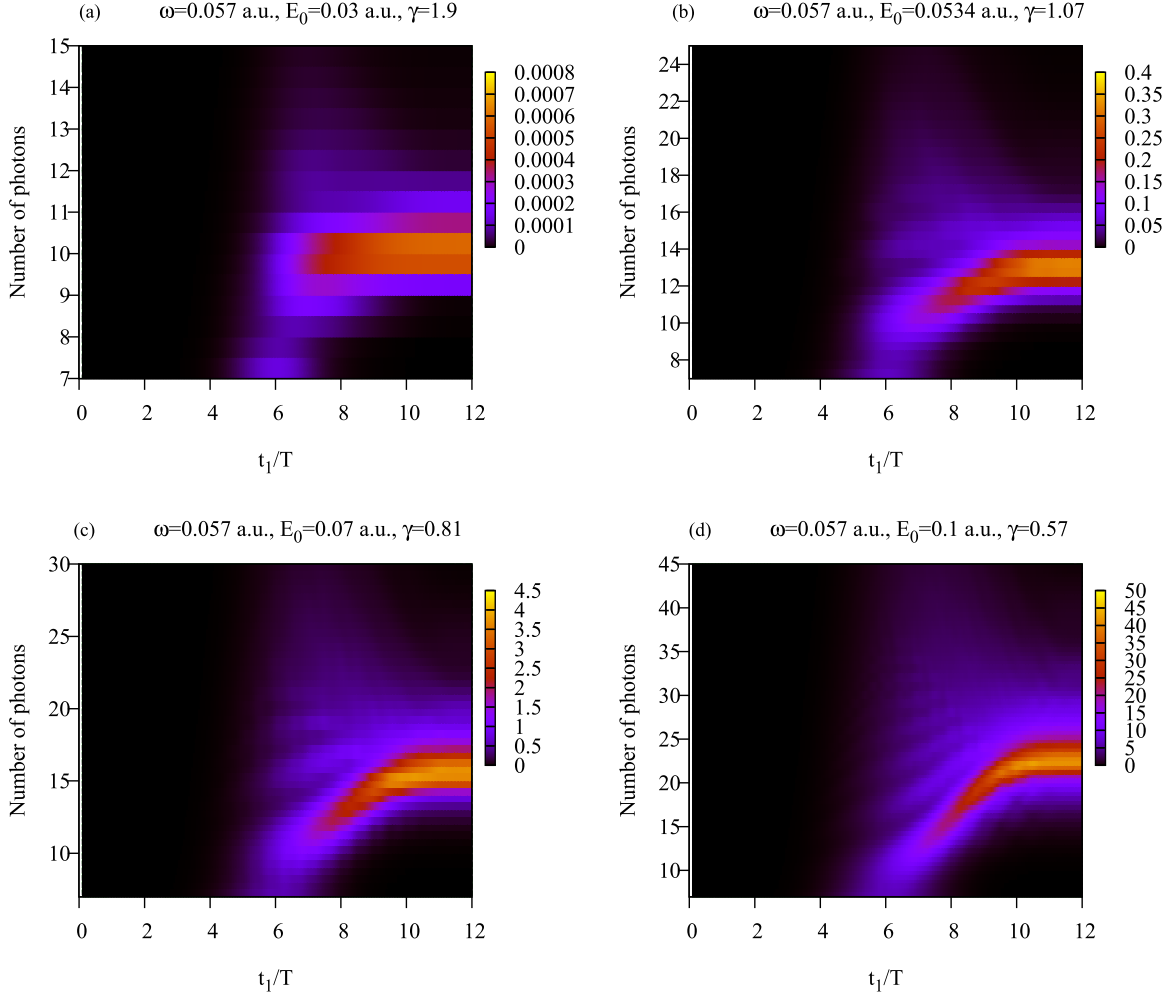


FIG. 5. Photon number distributions  $P(n, t)$  (scaled by a factor  $10^4$  for convenience) as functions of time for the atomic system governed by the short-range interaction (19).

Since we use Schrödinger representation, we added the field Hamiltonian  $\hat{H}_{\text{field}}$  on the right-hand side of Eq. (21). The interaction Hamiltonian  $\hat{H}_I$  in Eq. (21) has the same form as in Eq. (6) with the quantized vector potential given by Eq. (1), where, in the Schrödinger representation, we should put  $t = 0$  so that this operator is time independent. It is not difficult to see that, substituting expansion (11) into Eq. (21), using the asymptotic large- $N$  forms of the creation and annihilation operators, and projecting the result on a Fock state  $|m\rangle$ , we obtain a system of coupled equations (we use the dipole approximation again, neglecting spatial dependence of the vector potential):

$$i \frac{\partial \phi_m(t)}{\partial t} = \left( \hat{H}_{\text{atom}} + m\omega + \frac{1}{4c^2} A_0^2 \right) \phi_m + \frac{1}{2c} A_0 \cdot \hat{p} (\phi_{m+1} + \phi_{m-1}) + \frac{1}{8c^2} A_0^2 (\phi_{m+2} + \phi_{m-2}), \quad (22)$$

where  $A_0 = e_z \sqrt{\frac{8N\pi c^2}{\omega V}}$ . It is easy to see that if set  $\{\phi_m(t)\}$  solves Eq. (22) then the function  $\tilde{\Phi}(t) = \sum \phi_m(t) e^{im\omega t}$  solves

the TDSE equation for an atom in a monochromatic field:

$$i \frac{\partial \tilde{\Phi}(t)}{\partial t} = \left( \hat{H}_{\text{atom}} + \frac{1}{c} A_0 \cdot \hat{p} \cos \omega t + \frac{1}{2c^2} A_0^2 \cos^2 \omega t \right) \tilde{\Phi}(t), \quad (23)$$

We have therefore a map:

$$\Phi(t) = \sum_m \phi_m(t) \otimes |N+m\rangle \rightarrow \tilde{\Phi}(t) = \sum_m \phi_m(t) e^{im\omega t}, \quad (24)$$

which maps solutions  $\Phi(t)$  of the TDSE (21) which belongs to the Hilbert space  $\mathcal{H}_{\text{atom}} \otimes \mathcal{H}_{\text{field}}$  of the system atom + quantized field, on solutions of the atomic TDSE (23) which belongs to the Hilbert space  $\mathcal{H}_{\text{atom}}$ . This is not a one-to-one mapping, since if we know an arbitrary solution of the atomic TDSE  $\tilde{\Phi}(t)$ , it cannot be uniquely represented as an expansion  $\tilde{\Phi}(t) = \sum \phi_m(t) e^{im\omega t}$  to reconstruct preimage  $\Phi(t)$  uniquely. Rather, for a given solution of the atomic TDSE we can find many sets  $\{\phi_n(t)\}$  such that  $\tilde{\Phi}(t) = \sum \phi_m(t) e^{im\omega t}$ , therefore the mapping (24) is many to one, i.e., many solutions of the TDSE (21) can generally be mapped on a given solution of the



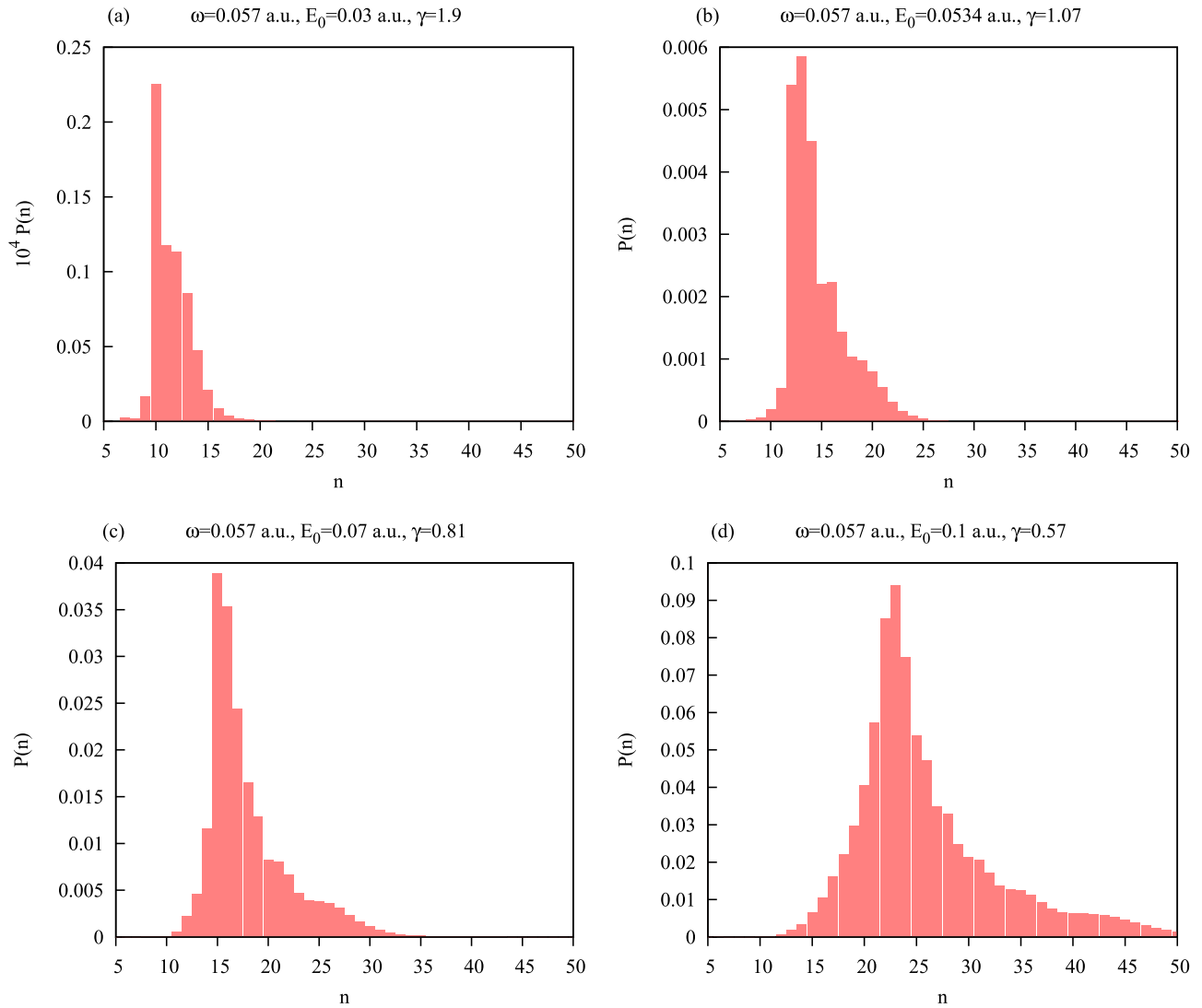


FIG. 6. Distribution  $P(n)$  for different effective field strengths for the hydrogen atom with the Coulomb potential obtained at the end of the pulse (17) with  $M = 12$  optical cycles.

atomic TDSE  $\tilde{\Phi}(t)$ . We can make this map a one-to-one map if we impose some additional requirements. If, for instance, we impose the requirement that dependence of all  $\{\phi_n(t)\}$  on time is particularly simple,  $\phi_n(t) = u_n e^{-i\epsilon t}$ , where  $u_n$  are time independent, and use outgoing waves boundary condition for  $\{u_n\}$ , the set of equations (22) reduces to the set of equations used in the Floquet method [28,44] for an eigenvector with the Floquet components  $\{u_n\}$  and quasienergy  $\epsilon$ . The usual procedure employed to arrive at the set of Floquet equations is based on the Floquet theorem [28], which states that for a Hamiltonian periodic in time with period  $T$ , TDSE allows a special set of solutions  $\Psi_s(t)$  which can be represented as  $\Psi_s(t) = e^{-i\epsilon_s t} u(t)$ , where  $u(t)$  is time periodic with period  $T$  and  $\epsilon_s$  is the complex quasienergy. The method is particularly well suited for the calculations of the total ionization rates, which are directly related to the imaginary parts of the quasienergies; it can also be applied to calculations of partial ionization rates, electron spectra for the process of the multiphoton ionization, or photon spectra for the high harmonic generation [44–52].

The present approach and the Floquet methods are therefore linked, though not equivalent. Once the outgoing wave boundary conditions are imposed on the Floquet components  $\{u_n\}$ , the mapping we described above is no longer from  $\mathcal{H}_{\text{atom}} \otimes \mathcal{H}_{\text{field}}$  to the atomic Hilbert space  $\mathcal{H}_{\text{atom}}$ . The outgoing wave boundary conditions make the Floquet components  $\{u_n\}$  exponentially grow at spatial infinity. The integrals defining partial ionization rates therefore diverge and must be suitably regularized. Various techniques allowing one to overcome this difficulty have been described in the literature. One can use an analytic continuation procedure [44,45]. Alternatively, the complex scaling transformation restoring the square integrability of the Floquet components can be applied [53,54]. This transformation makes the Hamiltonian non-Hermitian and leads to the complex symmetric non-Hermitian eigenvalue problem which can be solved using either matrix methods employing suitable basis sets or perturbatively [55]. A conceptually similar approach relies on the use of the complex absorbing potential (CAP) [52], which dampens outgoing waves at large distances and makes the Floquet eigenvectors

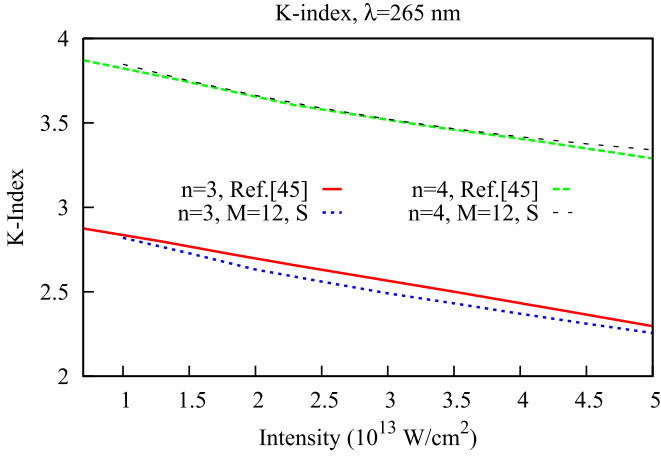


FIG. 7.  $K$  index of nonlinearity as a function of intensity for three- and four-photon absorption for a hydrogen atom (driving pulse wavelength of 265 nm).

square integrable. The presence of the CAP, of course, makes the Hamiltonian non-Hermitian. In the procedure we employ presently, we do not leave the Hilbert space  $\mathcal{H}_{\text{atom}} \otimes \mathcal{H}_{\text{field}}$  and the ordinary mathematical framework of quantum mechanics which presupposes use of Hermitian operators. We can apply, therefore, the standard quantum-mechanical prescriptions for calculation of the transition amplitudes.

Figure 7 shows a comparison of the calculations based on the present approach with the results of the Floquet calculation [45] for the multiphoton ionization of the hydrogen atom driven by the field with the wavelength of 265 nm. We compare results for the so-called  $K$  index of nonlinearity for different field intensities  $I$  and different numbers of absorbed photons  $n$ . In terms of the distribution function  $P(I, n)$  of absorbed photons (here we add explicit intensity dependence), which we compute, this index can be defined as  $K(I, n) = \frac{\partial \log P(I, n)}{\partial \log I}$ . To obtain  $P(I, n)$  we employed the procedure we described above (using the same envelope and pulse duration as for the results presented in Figs. 3–6). Figure 7 shows rather close agreement between the results of the two calculations.

### B. Initial coherent state

The formalism proposed in [30], which we used in the present work, can also be applied in the case when initial state of the field is different from the Fock state. Suppose we have a system atom + field prepared initially (in the distant past) in the state  $\Phi(0) = \phi_0 \otimes \sum C_N |N\rangle$ , where  $\phi_0$  is the initial atomic state, and absolute values of the coefficients  $C_N$  are peaked around some value  $N_0$ . We can use again the  $\theta$  representation of the photon Hilbert space, i.e., the mapping (2), which we can now write as  $|N_0 + m\rangle = e^{im\theta}$ . Under this mapping the initial state of the system atom + field becomes  $\phi_0 f(\theta)$ , where  $f(\theta) = \sum C_{N_0+m} e^{im\theta}$  is a known function of the angle  $\theta$ . In the limit of large  $N_0$  the QED propagator in this representation is known. It is given by the solution of Eq. (9), i.e., it is an atomic propagator depending on the angle  $\theta$  parametrically. We can, therefore, obtain the wave function of the atom + field system at the moment  $t$  as  $\Phi(t) = \hat{U}(t, 0, \theta) \phi_0 f(\theta)$ . Using the definition (3) of the

scalar product in the  $\theta$  representation, and going back to the more familiar representation of the Fock states, we can write  $\Phi(t) = \sum_m \phi_m(t) |N_0 + m\rangle$ , where the vector (belonging to the atomic Hilbert space)  $\phi_m(t)$  is

$$\phi_m(t) = \frac{1}{2\pi} \int_0^{2\pi} e^{-im\theta} \hat{U}(t, 0, \theta) \phi_0 f(\theta) d\theta. \quad (25)$$

In the case of the Fock initial state  $|N\rangle$  of the field we considered above,  $f(\theta) = 1$  and we recover Eq. (12). Another case of interest is ionization driven by the field in the coherent state. Such states are known to be the closest analogs of the classical electromagnetic waves, and can be represented as a superposition of the Fock states [32]:

$$|v\rangle = \exp^{-\frac{|v|^2}{2}} \sum_{N=0}^{\infty} c_N |N\rangle, \quad (26)$$

where  $c_N = \frac{v^N}{\sqrt{N!}}$ ,  $v = |v|e^{-i\phi}$  is an arbitrary complex number. Unlike the Fock states we considered above, the coherent states have nonzero expectation values of the field operators. In particular, from Eqs. (1) and (26) one obtains for the vector potential for the one-mode case we consider presently:  $\langle v | \hat{A}(\mathbf{r}, t) | v \rangle = \sqrt{\frac{8\pi|v|^2 c^2}{wV}} \mathbf{e}_z \cos(\omega t - \mathbf{k} \cdot \mathbf{r} + \phi)$ . To consider ionization driven by the coherent state (26) we could proceed as follows. We note, first that the absolute values of the coefficients  $C_N$  in (26) peak at the value  $N = \bar{N} = |v|^2$  [ $\bar{N}$  is the expectation value of the number of photons  $N$  in the coherent state (26)]. Simple calculation shows that in the vicinity of this maximum coefficients  $|c_N|$  can be represented as  $|c_{\bar{N}}| e^{-\frac{(N-\bar{N})^2}{4\bar{N}}}$ , and the coherent state (26) can then be approximately written as

$$|v\rangle \approx (2\pi\bar{N})^{-\frac{1}{4}} \sum_{m=-\infty}^{+\infty} e^{-i(\bar{N}+m)\phi - \frac{m^2}{4\bar{N}}} |\bar{N} + m\rangle, \quad (27)$$

where, of course, only the terms with small  $m$  actually contribute to the sum. Under the mapping (2), which we can now write as  $|\bar{N} + m\rangle = e^{im\theta}$ , the state vector (27) becomes a known function  $f(\theta)$ . Evolution of the system atom + field with the field in this initial state and the probabilities  $|\phi_m(t)|^2$  of finding the field in a particular Fock state at time  $t$  can now be found using Eq. (25). There is, however, a difference in the interpretations of the probabilities obtained in this way between the cases of the Fock and coherent initial states of the field. In the case of the initial Fock state  $|N\rangle$ , with fixed number of photons, projection of the time-evolved wave function on another Fock state  $|N_1\rangle$  with a different number of photons can be interpreted naturally as the probability of absorption or emission of  $N_1 - N$  photons. On the other hand, in the case of the initial coherent state with the expectation value  $\bar{N}$  of the number of photons, the number of photons is not fixed, with the dispersion proportional to  $\bar{N}^{\frac{1}{2}}$  [32]. The absolute fluctuations of the number of photons are, therefore, much larger for large  $\bar{N}$  than the average number of photons absorbed in the process of ionization; the latter number is defined essentially by the mean kinetic energy of the ionized electron and is of the order of 20–30 for the field parameters we consider. This makes the probabilities  $|\phi_m(t)|^2$  of finding the field in a particular Fock state less informative. On the other hand, the atomic characteristics, e.g., spectra of the

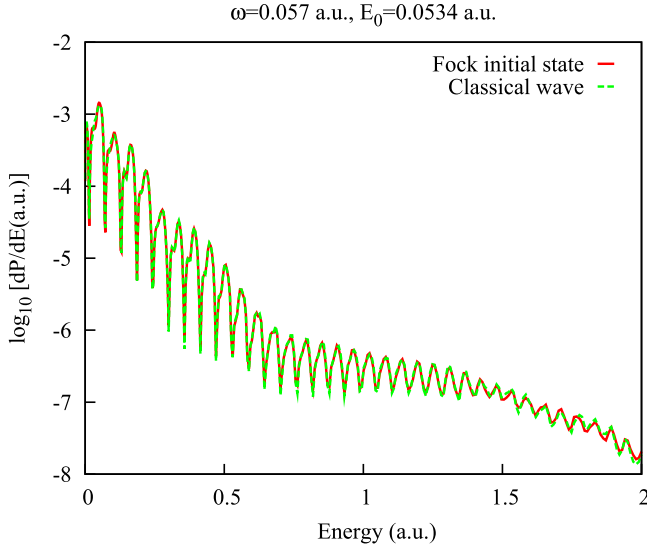


FIG. 8. Electron spectra obtained for the ionization driven by the field in the Fock state and the classical wave for the atomic system governed by the short-range potential (19).

ionized electrons, are pretty much identical in the calculations using Fock or coherent initial states. Indeed, as Eq. (13) shows, the effect of the undefined phase in the Fock state on the atomic density matrix is described by a procedure which amounts to averaging atomic density matrices obtained for coherent states with different phases of the field. For the long pulses we consider the effects due to the different carrier envelope phases (CEPs) can be safely neglected. To illustrate this statement, we show in Fig. 8 photoelectron energy spectrum obtained using expression (13) for the density matrix for the case of ionization driven by the field in a Fock state. The spectrum was calculated as  $\frac{dP}{dE} = \text{Tr} [\rho_{\text{atom}} \hat{Q}(E)] = \langle \Psi_E | \rho_{\text{atom}} | \Psi_E \rangle$ , where  $\hat{Q}(E) = |\Psi_E\rangle\langle\Psi_E|$  is a projector on a positive energy state  $\Psi_E$ , which as one can see from Eq. (13), reduces to a  $\theta$  average of the spectra obtained using a classical pulse with the same field strength and CEP of  $\theta$ . Results are compared to the spectrum obtained using a classical pulse and the particular CEP value of  $\pi/2$ . The pulse duration and envelope were the same we used above [envelope (17) with  $M = 12$  optical cycles].

A similar procedure, with only minor modifications, could be applied to the case when several modes of the field are present. This might be the case, for instance, when we consider an initial field state corresponding to a short pulse, such that envelope effects are important. Such an initial state might be represented as a superposition of several coherent states corresponding to different photon frequencies. The only difference that the inclusion of the several modes of the field would entail is additional computational effort: we would have to introduce a set of angle variables  $\theta$ , one for each mode of the field. We plan to report results of such a calculation elsewhere. It is, perhaps, the problem of the ionization driven by a short pulse, when the envelope and CEP effects are important, which most clearly demonstrates the difference of the present approach and the Floquet method. The Floquet method is very well suited for calculations of the atomic

ionization driven by a continuous wave (CW) radiation. The procedure we employ, on the other hand is, in essence, a solution of the evolution equations and can, therefore, be applied for the description of the short pulse duration effects, e.g., the CEP and pulse envelope effects on the electron and photon spectra.

### C. Perturbation theory approach

Equation (13) explains why results for the atomic characteristics obtained using the QED approach with the field in the Fock state and results based on the TDSE treating the field as a classical wave should agree. This fact can also be simply illustrated using the lowest order perturbation theory (LOPT). Consider, for instance, the process of one-photon absorption for the case of an atom initially in the ground state  $\phi_0$  with energy  $\varepsilon_0$ , which at the moment  $t = 0$  starts interacting with the one-mode field in the Fock state  $|N\rangle$ . We assume the photons in the mode are polarized in the  $z$  direction. Let the quantized field be described by the vector potential (1). The probability of detecting the system atom + field at time  $t$  in a state  $\phi_1 \otimes |N-1\rangle$  with electron energy  $\varepsilon_1$  is  $|a(t)|^2$ , where the amplitude  $a(t)$  is given by the QED LOPT formula (we use for simplicity a dipole approximation neglecting spatial dependence of the vector potential) [32]:

$$a(t) = -i \int_0^t \sqrt{\frac{2\pi N c^2}{wV}} e^{i(\varepsilon_1 - \omega - \varepsilon_0)\tau} \langle \phi_1 | \hat{p}_z | \phi_0 \rangle d\tau. \quad (28)$$

On the other hand, we could describe the field classically, using vector potential  $A(t) = A_0 \cos(\omega t + \phi)$ , where  $\phi$  is the CEP of the field. The quantum-mechanical LOPT based on the TDSE for an atom initially in the state  $\phi_0$  interacting with the classical field  $A(t)$  would give us for the amplitude of finding an electron at time  $t$  in the state  $\phi_1$  [56]

$$a_c(t) = -i \frac{A_0}{2} \int_0^t (e^{i(\varepsilon_1 - \omega - \varepsilon_0)\tau + i\phi} + e^{i(\varepsilon_1 + \omega - \varepsilon_0)\tau - i\phi}) \times \langle \phi_1 | \hat{p}_z | \phi_0 \rangle d\tau. \quad (29)$$

The second term inside the parentheses in Eq. (29) describes processes violating energy conservation; it is suppressed if we observe the system at a large enough moment of time  $t$  [56].

If we neglect this term and put  $A_0 = \sqrt{\frac{8\pi N c^2}{wV}}$  to ensure the same effective field strength, amplitudes (28) and (29) will be practically identical. The only difference is the appearance of the phase factor  $\phi$  in Eq. (29) which is absent in the amplitude (28) (phase is undefined in a Fock state). This phase factor, however, plays no role as long as we can neglect the second term inside the parentheses in Eq. (29) so that the two terms do not interfere, i.e., if we use a long enough pulse.

## V. CONCLUSIONS

We presented results of calculations of the probability distributions of the number of absorbed photons for atomic ionization driven by a field in the Fock state  $|N\rangle$  with a large number of photons  $N$  in the mode. We employed the method [30] which allowed us to consider the photon field and the field-atom interaction in a way following from the QED prescriptions in the limit  $N \rightarrow \infty$ .

We found probability distributions of absorbed photons for different field parameters, ranging from multiphoton to tunneling regimes of ionization. A comparison with the photon distributions following from the SFA formula (20) (as we mentioned, the interpretation of the distribution based on the SFA formula as a distribution of photons can be regarded with certain reservations) shows that the distributions we obtain are generally more narrow, with the expectation value  $\langle n \rangle$  of absorbed photons shifted towards smaller values of  $n$ . These differences are most pronounced for smaller field strengths. We performed calculations for both a model atom with the electron dynamics governed by the short-range interaction (19) and for a hydrogen atom with the Coulomb potential. Absorbed photons distribution in the Coulomb case exhibit a longer tail than the distribution obtained for the model atom with the short-range interaction. We attributed above the presence of this tail to the infinite-range character of the Coulomb forces. For the hydrogen atom the results we obtain agree well with the results of the calculations using the Floquet method.

In the calculations we performed an atom was described using the nonrelativistic quantum mechanical TDSE, which

means that we neglect both relativistic effects for the atomic electron and the processes due to the essentially many-body character of the electron field in QED (such as the pair creation processes). Neglect of all these effects is certainly justified for not too high field strengths and the photon frequency we considered in the paper. In fact we can, with relatively minor additional computational effort, lift the first of these restrictions and include the relativistic effects for the atomic electron as well. To this end we would need to solve the time-dependent Dirac equation (TDDE) instead of the TDSE in Eq. (14). A calculation based on such a strategy would bring us one step closer to the solution of a very complicated problem of a complete QED description of an atom in a strong field. Technically, such a calculation is certainly feasible given that various algorithms allowing one to solve the TDDE numerically have been described in the literature [57–59], and we plan to perform it in the future.

#### ACKNOWLEDGMENT

This work was supported by IBS (Institute for Basic Science) under IBS-R012-D1.

- 
- [1] H. R. Reiss, *J. Opt. Soc. Am. B* **7**, 574 (1989).
  - [2] A. Ludwig, J. Maurer, B. W. Mayer, C. R. Phillips, L. Gallmann, and U. Keller, *Phys. Rev. Lett.* **113**, 243001 (2014).
  - [3] F. Krausz and M. Ivanov, *Rev. Mod. Phys.* **81**, 163 (2009).
  - [4] C. T. L. Smeenk, L. Arissian, B. Zhou, A. Mysyrowicz, D. M. Villeneuve, A. Staudte, and P. B. Corkum, *Phys. Rev. Lett.* **106**, 193002 (2011).
  - [5] S. Chelkowski, A. D. Bandrauk, and P. B. Corkum, *Phys. Rev. Lett.* **113**, 263005 (2014).
  - [6] S. Chelkowski, A. D. Bandrauk, and P. B. Corkum, *Phys. Rev. A* **92**, 051401(R) (2015).
  - [7] I. A. Ivanov, J. Dubau, and K. T. Kim, *Phys. Rev. A* **94**, 033405 (2016).
  - [8] V. S. Popov, B. M. Karnakov, V. D. Mur, and S. G. Pozdnyakov, *Sov. Phys. JETP* **102**, 760 (2006).
  - [9] M. Klaiber and K. Z. Hatsagortsyan, *Phys. Rev. A* **90**, 063416 (2014).
  - [10] E. Yakaboylu, M. Klaiber, and K. Z. Hatsagortsyan, *Phys. Rev. A* **91**, 063407 (2015).
  - [11] N. Haram, I. Ivanov, H. Xu, K. T. Kim, A. Atia-tul-Noor, U. S. Sainadh, R. D. Glover, D. Chetty, I. V. Litvinyuk, and R. T. Sang, *Phys. Rev. Lett.* **123**, 093201 (2019).
  - [12] Simon Vendelbo Bylling Jensen, M. M. Lund, and L. B. Madsen, *Phys. Rev. A* **101**, 043408 (2020).
  - [13] D. B. Milošević, *Phys. Rev. A* **93**, 051402(R) (2016).
  - [14] J. Feldhaus, J. Arthur, and J. B. Hastings, *J. Phys. B: At. Mol. Opt. Phys.* **38**, S799 (2005).
  - [15] C. Gutt, L.-M. Stadler, S. Streit-Nierobisch, A. P. Mancuso, A. Schropp, B. Pfau, C. M. Günther, R. Könnecke, J. Gulden, B. Reime *et al.*, *Phys. Rev. B* **79**, 212406 (2009).
  - [16] L. Fang, M. Hoener, O. Gessner, F. Tarantelli, S. T. Pratt, O. Kornilov, C. Buth, M. Gühr, E. P. Kanter, C. Bostedt *et al.*, *Phys. Rev. Lett.* **105**, 083005 (2010).
  - [17] Z. Zhou and Shih-I Chu, *Phys. Rev. A* **87**, 023407 (2013).
  - [18] I. A. Ivanov, *Phys. Rev. A* **96**, 013419 (2017).
  - [19] T. Tajima and G. Mourou, *Phys. Rev. Spec. Top. Accel. Beams* **5**, 031301 (2002).
  - [20] G. A. Mourou, T. Tajima, and S. V. Bulanov, *Rev. Mod. Phys.* **78**, 309 (2006).
  - [21] Y. Salamin, S. Hu, K. Hatsagortsyan, and C. Keitel, *Phys. Rep.* **427**, 41 (2006).
  - [22] F. Fillion-Gourdeau, E. Lorin, and A. D. Bandrauk, *Phys. Rev. A* **86**, 032118 (2012).
  - [23] F. Fillion-Gourdeau, E. Lorin, and A. D. Bandrauk, *Phys. Rev. Lett.* **110**, 013002 (2013).
  - [24] L. V. Keldysh, *Sov. Phys. JETP* **20**, 1307 (1965).
  - [25] F. H. M. Faisal, *J. Phys. B* **6**, L89 (1973).
  - [26] H. R. Reiss, *Phys. Rev. A* **22**, 1786 (1980).
  - [27] S. V. Popruzhenko, *J. Phys. B: At. Mol. Opt. Phys.* **47**, 204001 (2014).
  - [28] A. Maquet, Shih-I Chu, and W. P. Reinhardt, *Phys. Rev. A* **27**, 2946 (1983).
  - [29] E. M. Lifshitz and V. B. Berestetskii, *Quantum Electrodynamics* (Pergamon, Oxford, 1982).
  - [30] I. Bialynicki-Birula, *Acta Phys. Austriaca, Suppl.* **XVIII**, 111 (1977).
  - [31] I. I. Sobelman, *Introduction to the Theory of Atomic Spectra* (Pergamon, Oxford, 1972).
  - [32] L. Mandel and E. Wolf, *Optical Coherence and Quantum Optics* (Cambridge University Press, Cambridge, UK, 1995).
  - [33] A. Messiah, *Quantum Mechanics* (John Wiley & Sons, New York, 1966).
  - [34] N. N. Bogoliubov and D. V. Shirkov, *Introduction to the Theory of Quantized Fields* (John Wiley & Sons, New York, 1959).
  - [35] V. S. Popov, *Phys. Usp.* **47**, 855 (2004).
  - [36] I. A. Ivanov, *Phys. Rev. A* **83**, 023421 (2011).
  - [37] I. A. Ivanov and A. S. Kheifets, *Phys. Rev. A* **96**, 013408 (2017).

- [38] I. A. Ivanov and A. S. Kheifets, *Phys. Rev. A* **85**, 013406 (2012).
- [39] I. A. Ivanov, A. S. Kheifets, and V. V. Serov, *Phys. Rev. A* **86**, 063422 (2012).
- [40] I. A. Ivanov, *Phys. Rev. A* **90**, 013418 (2014).
- [41] W. E. Lamb, *Phys. Rev.* **85**, 259 (1952).
- [42] A. M. Perelomov, V. S. Popov, and M. V. Terentiev, *Sov. Phys. JETP* **23**, 924 (1966).
- [43] V. S. Popov, *J. Exp. Theor. Phys.* **91**, 48 (2000).
- [44] R. M. Potvliege and R. Shakeshaft, *Phys. Rev. A* **38**, 4597 (1988).
- [45] R. M. Potvliege and R. Shakeshaft, *Phys. Rev. A* **38**, 1098 (1988).
- [46] P. G. Burke, P. Francken, and C. J. Joachain, *J. Phys. B* **24**, 761 (1991).
- [47] M. S. Pindzola and M. Dorr, *Phys. Rev. A* **43**, 439 (1991).
- [48] P. G. Burke, J. Colgan, D. H. Glass, and K. Higgins, *J. Phys. B* **33**, 143 (2000).
- [49] S.-I. Chu and D. A. Telnov, *Chem. Phys. Lett.* **264**, 466 (1997).
- [50] S.-I. Chu and D. A. Telnov, *Phys. Rep.* **390**, 1 (2004).
- [51] D. A. Telnov and Shih-I Chu, *Phys. Rev. A* **71**, 013408 (2005).
- [52] T. Tsogbayar and M. Horbatsch, *J. Phys. B* **46**, 245005 (2013).
- [53] E. Balslev and J. M. Combes, *Commun. Math. Phys.* **22**, 280 (1971).
- [54] S.-I. Chu and W. P. Reinhardt, *Phys. Rev. Lett.* **39**, 1195 (1977).
- [55] D. A. Telnov and Shih-I Chu, *Phys. Rev. A* **61**, 013408 (1999).
- [56] N. B. Delone and V. P. Krainov, *Multiphoton Processes in Atoms* (Springer-Verlag, Berlin, 1994).
- [57] T. Kjellsson, S. Selstø, and E. Lindroth, *Phys. Rev. A* **95**, 043403 (2017).
- [58] I. A. Ivanov, *Phys. Rev. A* **91**, 043410 (2015).
- [59] D. A. Tumafov, D. A. Telnov, G. Plunien, V. A. Zaytsev, and V. M. Shabaev, [arXiv:2005.13613](https://arxiv.org/abs/2005.13613).